cylinders–Nonabsorbing and absorbing," *J. Acoust. Soc. Amer.*, vol. 62, pp. 513-517, Sept. 9, 1977.
[23] H. Uberall, "Surface waves in acoustics," in *Physical Acoustics, Principles and Methods*, vol. X, W. P. Mason, Ed. New York: Academic, 1973.
[24] H. H. Uhlig, *The Corrosion Handbook*. New York: Wiley, 1948.
[25] W. Clayman, ATS Lab., Inc., private communication.
[26] *Science*, vol. 211, pp. 556-557, Feb. 1981.
[27] W. G. Neubauer and L. R. Dragonette, "Observation of waves radiated from circular cylinders caused by an incident pulse," *J. Acoust. Soc. Amer.*, vol. 48, pp. 1135-1149, 1970.
[28] W. G. Neubauer, "Observation of acoustic radiation from plane and curved surfaces," in *Physical Acoustics, Principles and Methods*, vol. X, W. P. Mason, Ed. New York: Academic, 1973, pp. 61-126.
[29] D. Brill and H. Uberall, "Acoustic waves transmitted through solid elastic cylinders," *J. Acoust. Soc. Amer.*, vol. 50, p. 391, Fig. 10, 1971.

Maximum Likelihood Reconstruction for Emission Tomography

L. A. SHEPP AND Y. VARDI

Abstract–**Previous models for emission tomography (ET) do not distinguish the physics of ET from that of transmission tomography. We give a more accurate general mathematical model for ET where an unknown emission density $\lambda = \lambda(x, y, z)$ generates, and is to be reconstructed from, the number of counts $n^*(d)$ in each of D detector units d. Within the model, we give an algorithm for determining an estimate $\hat{\lambda}$ of λ which maximizes the probability $p(n^*|\lambda)$ of observing the actual detector count data n^* over all possible densities λ.**

Let independent Poisson variables $n(b)$ with unknown means $\lambda(b)$, $b = 1, \cdots, B$ represent the number of unobserved emissions in each of B boxes (pixels) partitioning an object containing an emitter. Suppose each emission in box b is detected in detector unit d with probability $p(b, d)$, $d = 1, \cdots, D$ with $p(b, d)$ a one-step transition matrix, assumed known. We observe the total number $n^* = n^*(d)$ of emissions in each detector unit d and want to estimate the unknown $\lambda = \lambda(b)$, $b = 1, \cdots, B$. For each λ, the observed data n^* has probability or likelihood $p(n^*|\lambda)$. The EM algorithm of mathematical statistics starts with an initial estimate λ^0 and gives the following simple iterative procedure for obtaining a new estimate $\hat{\lambda}^{\text{new}}$ from an old *estimate* $\hat{\lambda}^{\text{old}}$, to obtain $\hat{\lambda}^k, k = 1, 2, \cdots,$

$$\hat{\lambda}^{\text{new}}(b) = \hat{\lambda}^{\text{old}}(b) \sum_{d=1}^{D} \frac{n^*(d)p(b,d)}{\sum_{b'=1}^{B} \hat{\lambda}^{\text{old}}(b')p(b',d)}, \quad b = 1, \cdots, B.$$

We show that the likelihood strictly increases at each step (unless it is already a maximum), $p(n^*|\lambda^k) \geq p(n^*|\hat{\lambda}^{k-1})$, $k \geq 1$; the total number $\Sigma \hat{\lambda}(b)$ of estimated counts is equal to the total number $\Sigma n^*(d)$ of observed counts at each step $\hat{\lambda}^k$, $k \geq 1$; $\hat{\lambda}^k$ converges as $k \to \infty$ to an estimate $\hat{\lambda}^\infty$ which has maximum likelihood; $\hat{\lambda}^k(b) \geq 0$; $l(\lambda) = \log p(n^*|\lambda)$ is concave.

We show by simulation that this algorithm reduces the statistical noise artifact over conventional convolution backprojection algorithms without introducing excessive smoothing. This is important because statistical noise is a major limiting factor in emission tomography. The method is generally applicable to any design geometry (single or multiring), to single or double photon emission tomography, and can incorporate timing information and correct for positron range and angle effects in a simple way. We discuss methods to speed convergence of the computation.

Mansucript received May 14, 1982.
The authors are with Bell Laboratories, Murray Hill, NJ 07974.

I. Introduction

In emission tomography (ET) [1]-[3], a compound containing a radioactive isotope is introduced into the body and forms an unknown emitter density $\lambda(x, y z) \geq 0$ under the body's metabolism. Emissions then occur according to a Poission process with rate $\lambda(x, y, z)$. In the usual case of positron emitter, the positron emitted finds a nearby electron and annihilates with it. A pair of X-ray photons fly off from the point of annihilation at the speed of light in opposite directions along a line which is uniformly distributed in angle. There is an array of discrete detector elements surrounding the body and the two photons are detected in coincidence by a pair of detector elements defining a detector unit, or detector tube, d. It is known only that somewhere along the length of the tube d the annihilation took place. The case of single X-ray photon emitter is similar, but here collimation is used to define the detector tube.

The measured data are then $n^*(1), \cdots, n^*(D)$, where $n^*(d)$ is the total number of coincidences counted in the dth detector tube, and the problem is to estimate the emission density $\lambda(x, y, z)$ from the data n^*. For purpose of display and for purpose of machine computations, we discretize the density λ into boxes $b = 1, \cdots, B$, at the outset. Thus, in each box b there is an unknown count $n(b)$ with mean $\lambda(b) = En(b)$, $b = 1, \cdots, B$ and our problem is to estimate $\lambda(b)$, or roughly, to guess the true unobserved count $n(b)$ in each box, from the observed data $n^*(d)$, $d = 1, \cdots, D$.

A (nearly perfect) mathematical model of the above physics is the following one. Denote by $\lambda(b)$ the integral of $\lambda(x, y, z)$ over box b and let a Poisson distributed number $n(b)$ with

0278-0062/82/1000-0113$00.75 © 1982 IEEE

mean $\lambda(b)$ be generated independently in each box,

$$P(n(b) = k) = e^{-\lambda(b)} \frac{\lambda(b)^k}{k!}, \quad k = 0, 1, \cdots. \tag{1.1}$$

Suppose that each emission in box b is detected in tube d with known probability

$$p(b,d) = P(\text{detected in } d \mid \text{emitted in } b) \tag{1.2}$$

so that $p(b,d) \geqslant 0$. Thus, the probability of an emission in b being detected at all is given by

$$p(b) = \sum_{d=1}^{D} p(b,d) \leqslant 1. \tag{1.3}$$

The transition matrix $p(b,d)$ is assumed exactly known from the detector array geometry. After each emission moves to some detector tube, or is missed and undetected, there is a known total number $n^*(d)$ of counts in each tube $d = 1, \cdots, D$. The probability $P(\boldsymbol{n}^* \mid \boldsymbol{\lambda})$ of observing $n^*(d)$, $d = 1, \cdots, D$ is a function $L(\boldsymbol{\lambda})$ of the unknown rate $\boldsymbol{\lambda} = \lambda(b)$, $b = 1, \cdots, B$. We want to choose an estimate $\hat{\boldsymbol{\lambda}}$ of $\boldsymbol{\lambda}$ to maximize $L(\boldsymbol{\lambda})$. Such an estimate $\hat{\boldsymbol{\lambda}}$ is called a maximum likelihood estimate of $\boldsymbol{\lambda}$ given $\boldsymbol{n}^*$.

We begin by observing that it is much simpler and involves no loss of generality to assume that equality holds in (1.3). Indeed, if we let $\lambda'(b)$ represent the mean of $n'(b)$ = the number of emissions in b *which are actually detected in some detector*, then $p'(b,d) = p(b,d)/p(b)$ is the (conditional) probability that a *detected* photon emitted in b is detected in d and satisfies

$$\sum_{d=1}^{D} p'(b,d) = 1. \tag{1.3}'$$

Since a Poisson process with rate $\lambda'(b)$, $b = 1, \cdots, B$ is obtained from the original process $\lambda(b)$, $b = 1, \cdots, B$ by thinning according to detection, it is clear ([4] and Section II) that $\lambda'(b) = \lambda(b)p(b)$ and $p(n^* \mid \lambda) = p(n^* \mid \lambda')$. Thus, if $\hat{\boldsymbol{\lambda}}$ is a maximum likelihood estimate of $\boldsymbol{\lambda}$ then $\hat{\boldsymbol{\lambda}}'$ is a maximum likelihood estimate of $\boldsymbol{\lambda}' = \boldsymbol{\lambda}'(b) = \lambda(b)p(b)$ and conversely. Henceforth, we will assume that equality holds in (1.3). This is equivalent to thinking of $\lambda(x,y,z)$ as the density of emitted counts *which are detected.*

The reader may have observed that the above model is only nearly exact. The assumption that emissions follow Poisson statistics (1.1) seems beyond challenge, but there is ambiguity in the discretization into boxes and how $p(b,d)$ is to be determined. This ambiguity seems to be unavoidable and is certainly less crude than the approximation required to force the model of transmission tomography to fit the emission case as we will see. We will discuss in Sections II and III how $p(b,d)$ is to be determined.

We also neglected two assumptions in describing the physics. First, the positron has nonzero (a few mm) range before annihilation and the angle between the paths of the two photons is (a few degrees) less than 180° unless the positron is exactly at rest. However, we show in Section III that these assumptions can readily be incorporated into the choice of $p(b,d)$ and so may not be a serious problem. The second assumption was to neglect the fact that either or both photons can be deflected (a scattering error), or two nearly simultaneous annihilations can have exactly one photon detected (an accidental error). In each case the wrong detector tube gets incremented. Scattered and accidental count errors are well-known [1]-[3], and depend on the *absorption* density of the body and so cannot be incorporated into $p(b,d)$ in an exact way. Ideally, these errors should be eliminated in the physical measurement procedure, e.g., by energy discrimination of scattered counts and by timing discrimination of accidental counts. We shall simply be forced to ignore these problems and to assume that the *only source of difficulty* is in the *statistical fluctuations* in the counting statistics $\boldsymbol{n}^*$.

We begin the mathematical discussion by noting that the variables $n^*(d)$ are independent and Poisson with expectation $\lambda^*(d)$,

$$\lambda^*(d) = En^*(d) = \sum_{b=1}^{B} \lambda(b)p(b,d). \tag{1.4}$$

This fact, pointed out by Snyder [4], is seen immediately by noting that

$$n^*(d) = \sum_{b=1}^{B} n(b,d) \tag{1.5}$$

where $n(b,d)$ is the number of emissions in b detected in d. Indeed, the variables $n(b,d)$, $b = 1, \cdots, B$, $d = 1, \cdots, D$ are all mutually independent Poisson variables and so the disjoint sums in (1.5) are also independent and Poisson and (1.4) follows from (1.5) by taking expectations. The maximum value of $\exp(-\lambda)\lambda^n/n!$ over λ occurs at $\lambda = n$ so that the maximum likelihood estimator of $\lambda^*(d)$ given $n^*(d)$ is $\hat{\lambda}^*(d) = n^*(d)$, $d = 1, \cdots, D$. Now one might attempt to simply solve the simultaneous equations (1.4) for $\boldsymbol{\lambda} = \lambda(b)$ with $n^*(d)$ substituted for $\lambda^*(d)$, and $p(b,d)$ known, to obtain an estimate of $\boldsymbol{\lambda}$. Because it is approximately true that, for a single ring planar detector array,

$$\lambda^*(d) = \iint_{T(d)} \lambda(x,y)\, dx\, dy \tag{1.6}$$

where $T(d)$ is the dth tube and $p(b,d)$ is approximately constant along $T(d)$, (1.4) are more or less the same equations as in transmission tomography and that mathematical apparatus is usually used in ET [1]-[3]. (See also the remark at the end of Appendix I in this connection.)

We emphasize that there are two problems with this approach. The first, and less serious, problem is that $\lambda^*(d)$ is actually given by

$$\lambda^*(d) = \iint_{T(d)} \lambda(x,y)p((x,y),d)\, dx\, dy \tag{1.6}'$$

where $p((x,y),d)$ is the probability that a line through (x,y), at a uniformly distributed random angle, will lie inside tube $T(d)$. The function $p((x,y),d)$ is a complicated function of (x,y) inside $T(d)$, vanishing along the sides of the tube

$T(d)$ and not constant. Thus, it is not quite correct to use an algorithm developed for strip integrals (1.6) to invert (1.6)'. Indeed, in the experiments of Section IV where ET data are generated instead of transmission data, as described there, subtle artifacts are apparent which seem to be explainable on the basis of the discrepancy between (1.6) and (1.6)'. Nevertheless, because of the low resolution ($\approx$1 cm) obtained to date in ET, this problem hardly justifies much effort to correct, since the artifacts introduced are small. The second problem with using transmission algorithms to invert (1.4) for $\boldsymbol{\lambda}$ is that at the low count rates intrinsic to ET, this procedure amplifies the statistical noise in the estimate of $\boldsymbol{\lambda}$ over that obtained by the maximum likelihood procedure. We show in Section IV by using simulation, that the maximum likelihood procedure results in a reconstruction $\hat{\boldsymbol{\lambda}}$ which has evidently less noise without excessive smoothing. Our explanation for this increased noise effectiveness is that $n^*(d) \approx 10^2$ or 10^3 and (1.4) are nearly singular.

II. Maximum Likelihood Estimation of $\boldsymbol{\lambda}$ Given n^*

Since the variables $n(b,d)$ = the number of emissions in box b detected in tube d are independent Poisson variables with mean

$$En(b,d) = \lambda(b,d) = \lambda(b)p(b,d) \tag{2.1}$$

the likelihood function is given by

$$L(\boldsymbol{\lambda}) = P(\boldsymbol{n}^*|\boldsymbol{\lambda}) = \sum_A \prod_{\substack{b=1,\cdots,B \\ d=1,\cdots,D}} e^{-\lambda(b,d)} \frac{\lambda(b,d)^{n(b,d)}}{n(b,d)!} \tag{2.2}$$

where the sum is over all arrays A of $n(b,d)$'s with

$$n^*(d) = n(\cdot,d) \overset{\text{def}}{=} \sum_{b=1}^{B} n(b,d), \qquad d = 1,\cdots,D \tag{2.3}$$

observed counts in the dth detector tube. Note also that

$$n(b) = n(b,\cdot) \overset{\text{def}}{=} \sum_{d=1}^{D} n(b,d) \tag{2.4}$$

is the (unobservable) number of emissions in the bth box. The sum in (2.2) is very complicated, but we will show that

$$l(\boldsymbol{\lambda}) = \log L(\boldsymbol{\lambda}) \tag{2.5}$$

is concave as a function of $\boldsymbol{\lambda} = \lambda(1),\cdots,\lambda(B)$ because of special properties of the Poisson model. We first show that the partial derivative of $l(\boldsymbol{\lambda})$ with respect to $\lambda(b_0)$ is

$$\frac{\partial l(\boldsymbol{\lambda})}{\partial \lambda(b_0)} = -1 + \sum_{d=1}^{D} \frac{n^*(d)p(b_0,d)}{\sum_{b'=1}^{B} \lambda(b')p(b',d)}. \tag{2.6}$$

By direct differentiation in (2.2),

$$\frac{\partial L(\boldsymbol{\lambda})}{\partial \lambda(b_0)} = \sum_A \left\{ \prod_{\substack{b=1,\cdots,B \\ d=1,\cdots,D}} e^{-\lambda(b,d)} \frac{\lambda(b,d)^{n(b,d)}}{n(b,d)!} \right\} \cdot \left\{ -1 + \frac{1}{\lambda(b_0)} \sum_{d=1}^{D} n(b_0,d) \right\}. \tag{2.7}$$

By definition of A on (2.2), the conditional expectation

$$E[n(b_0)|\boldsymbol{n}^*,\boldsymbol{\lambda}] = \frac{1}{P(\boldsymbol{n}^*|\boldsymbol{\lambda})} \sum_A \prod_{\substack{b=1,\cdots,B \\ d=1,\cdots,D}} e^{-\lambda(b,d)} \cdot \frac{\lambda(b,d)^{n(b,d)}}{n(b,d)!} n(b_0). \tag{2.8}$$

Comparing the second term in (2.7) with (2.8) and using (2.4) we get

$$\begin{aligned} \frac{\partial l(\boldsymbol{\lambda})}{\partial \lambda(b_0)} &= \frac{1}{L(\boldsymbol{\lambda})} \frac{\partial L(\boldsymbol{\lambda})}{\partial \lambda(b_0)} = \frac{1}{P(\boldsymbol{n}^*|\boldsymbol{\lambda})} \\ &\quad \cdot \left\{ -P(\boldsymbol{n}^*|\boldsymbol{\lambda}) + \frac{P(\boldsymbol{n}^*|\boldsymbol{\lambda})}{\lambda(b_0)} E[n(b_0)|\boldsymbol{n}^*,\boldsymbol{\lambda}] \right\} \\ &= -1 + \frac{1}{\lambda(b_0)} \sum_{d=1}^{D} E[n(b_0,d)|\boldsymbol{n}^*,\boldsymbol{\lambda}]. \end{aligned} \tag{2.9}$$

Now because of (2.3) and the fact that $n(b,d)$ are all mutually independent, the dth term in the sum in (2.9) is

$$\begin{aligned} E[n(b_0,d)|\boldsymbol{n}^*,\boldsymbol{\lambda}] &= E[n(b_0,d)|n^*(d),\boldsymbol{\lambda}] \\ &= \frac{n^*(d)\lambda(b_0,d)}{\sum_{b'=1}^{B} \lambda(b',d)} \end{aligned} \tag{2.10}$$

since for independent Poisson variables X, Y with means λ_X, λ_Y, $E[X|X+Y] = (X+Y)\lambda_X/(\lambda_X+\lambda_Y)$. Equation (2.6) now follows from (2.1) and (2.10). From (2.6) we see that

$$\frac{\partial^2 l(\boldsymbol{\lambda})}{\partial \lambda(b_0)\partial \lambda(b_1)} = -\sum_{d=1}^{D} \frac{n^*(d)p(b_0,d)p(b_1,d)}{\left[\sum_{b'=1}^{B} \lambda(b')p(b',d)\right]^2}. \tag{2.11}$$

It follows immediately from (2.11) that for any $z(1),\cdots,z(B)$

$$\sum_{b_0=1}^{B} \sum_{b_1=1}^{B} z(b_0)z(b_1) \frac{\partial^2 l(\boldsymbol{\lambda})}{\partial \lambda(b_0)\partial \lambda(b_1)} = -\sum_{d=1}^{D} n^*(d)c^2(d)$$

$$c(d) = \frac{\sum_{b=1}^{B} z(b)p(b,d)}{\sum_{b'=1}^{B} \lambda(b')p(b',d)} \tag{2.12}$$

and since $n^*(d)c^2(d) \geq 0$, the quadratic form is negative semidefinite so that $l(\boldsymbol{\lambda})$ is concave.

We now describe an iterative scheme, based on the EM algorithm [5, Appendix I] for maximizing l. We start the algorithm with an initial guess $\lambda^0(b)$ satisfying $\lambda^0(b) > 0$, $b = 1,\cdots,B$, and then in each iteration, if $\hat{\lambda}^{\text{old}}(b)$ denotes the current estimate of $\lambda(b)$, the new estimate is defined as

$$\hat{\lambda}^{\text{new}}(b) = \hat{\lambda}^{\text{old}}(b) \sum_{d=1}^{D} \frac{n^*(d)p(b,d)}{\sum_{b'=1}^{B} \hat{\lambda}^{\text{old}}(b')p(b',d)} \qquad b = 1,\cdots,B. \tag{2.13}$$

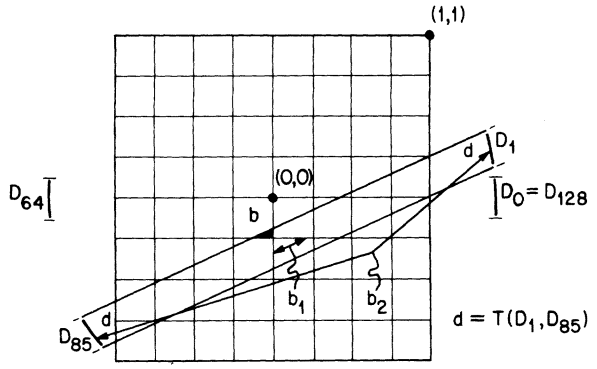

Fig. 1. There are $B \approx \pi/4 \times 128^2$ boxes b inside the circle of radius 1 (patient circle); each box has side 2/128. The detector circle of radius $\sqrt{2}$ has 128 equidivisions into detectors. A pair of detectors, such as D_1, D_{85}, defines a detector unit, or a tube, d.

(The algorithm could never lead to a quotient of a positive numerator divided by a zero denominator; zero divided by zero is defined as zero.) In the implementation of (2.13), discussed in Section III, we usually use a uniform constant as the initial estimate $\hat{\lambda}^0$. As a point of philosophical interest, the choice of the initial estimate $\hat{\lambda}^0$ is somewhat akin to the choice of a Bayes prior but there is actually no prior measure. For continuity we defer to Appendix I the proof, familiar from the EM algorithm [5], that in each step the new estimate $\hat{\lambda}^{\text{new}}$ is an improvement over the old estimate $\hat{\lambda}^{\text{old}}$:

$$L(\hat{\boldsymbol{\lambda}}^{\text{new}}) \geq L(\hat{\boldsymbol{\lambda}}^{\text{old}}), \tag{2.14}$$

with equality if and only if $L(\hat{\boldsymbol{\lambda}}^{\text{old}}) = \max_{\boldsymbol{\lambda}} L(\boldsymbol{\lambda})$. It then follows from the concavity of $\log L(\boldsymbol{\lambda})$ that all maxima of $L(\boldsymbol{\lambda})$ are global maxima and so the iteration scheme (2.13) gives a sequence

$$\hat{\boldsymbol{\lambda}}^0, \hat{\boldsymbol{\lambda}}^1, \cdots \tag{2.15}$$

which converges to a global maximum likelihood estimator $\hat{\boldsymbol{\lambda}}^\infty$. Of course if the maximum of $L(\boldsymbol{\lambda})$ is not unique then by the concavity of $\log L(\boldsymbol{\lambda})$ any convex combination of maxima is a maximum and $\hat{\boldsymbol{\lambda}}^\infty$ depends on the initial choice $\hat{\boldsymbol{\lambda}}^0$.

It is immediate from (2.13) that

$$\sum_{b=1}^{B} \hat{\lambda}^{\text{new}}(b) = \sum_{d=1}^{D} n^*(d) \quad \text{and} \quad \hat{\lambda}^{\text{new}}(b) \geq 0 \tag{2.16}$$

so that the true total number of counts is automatically preserved in the estimate $\hat{\boldsymbol{\lambda}}^{\text{new}}$, and $\hat{\lambda}^{\text{new}}(b) \geq 0$ at each stage. This does not hold for the conventional algorithms of transmission tomography adapted to ET.

III. Choice of $p(b, d)$

How should we actually choose $p(b, d)$, the probability that an emission in b is detected in d (see Fig. 1)? Detector unit d may be thought of as a tube defined by the two detectors D_1 and D_{85} at opposite ends of the strip $T = T(D_1, D_{85})$ in Fig. 1 and so $p(b, d)$ is a measure of the angle-of-view of box b into tube d and is the weighted average value of $p((x, y), d)$ [defined after (1.6)'] over the box b, the weight function being $\lambda(x, y)$. Unfortunately, $\lambda(x, y)$ is unknown and so $p(b, d)$ is impossible to compute exactly. Various approximations suggest themselves; what must be made is a choice of the weighting distribution in computing the average of $p((x, y), d)$. Fortunately, we find in Section IV that two such choices lead to reconstructions which do not differ significantly in our simulation.

We show next how it is easy to incorporate known facts or assumptions about positron range and angle to modify $p(b, d)$ to correct for these effects. Indeed suppose it is assumed that positrons range uniformly over a circle of fixed radius ρ (which may be varied) after emission and then annihilate. Then in Fig. 1 there is a certain calculable probability $p(b_1, d)$ that a positron emitted say uniformly in b_1 will range into and cause a count in d. More generally, a positron emitted in b_2 in Fig. 1 may have nonzero velocity and due to conservation of momentum have angle uniformly distributed over some interval depending on the range location, leading at least in principle to an estimate for $p(b_2, d)$. We have not tried this but just want to point out its feasibility and easy incorporation into the Poisson model. It is also worth pointing out that, if as predicted by Ter-Pogossian [3], it soon becomes possible by time-of-flight measurements to know to within say 6 cm where along $T(d)$ the firing took place then this information can also be used. Indeed we could partition each tube d into subtubes d_j, $j = 1, \cdots, m$ and compute probabilities $p(b, d_j)$ that an emission in b be detected in detector tube d_j. No essential change in the algorithm (2.13) need be used. It should be mentioned, however, that each of these corrections or modifications costs additional computational effort because the array of nonzero $p(b, d)$ values is made greater in each case and the computational effort depends on how many of the $p(b, d)$ constants are nonzero.

How should the computation (2.13) proceed for maximum efficiency? Ideally the constants $p(b, d)$ should be computed once and stored but since there are BD of these and each of B and D is about 10^4, this is somewhat inconvenient. Storing the nonzero $p(b, d)$ values is more convenient but the programming demands more effort. We decided to compute $p(b, d)$ anew, on the fly, each time it is needed, as is clear in the program supplied in Appendix II. For this purpose we used $p(b, d)$'s which were easy to calculate, for most of our runs. We chose $p(b, d) = (2nR)^{-1} \times$ (width of the intersection of the circle of radius R about the center of b and the strip defined by the tube d), where R is a parameter which we usually take to be the radius of the inscribed circle to b, and n is the number of detector elements around the detector circle. Note $\Sigma_{d=1}^{D} p(b, d) = 1$ and $p(b, d)$ is exact for the following imaginary positron range physics. Suppose a positron emitted in b immediately runs to the center of b then runs a distance ρ with probability density $P(\rho) = \rho/(R\sqrt{R^2 - \rho^2})$, $0 < \rho < R$, in a random direction, to reach a point Q in the disk of radius R about the center of b. Upon reaching Q the positron annihilates and the photon pair chooses a line through Q, not at random, but uniformly over the n tube directions. As we see in the simulations of Section IV this choice of $p(b, d)$ produces remarkably accurate reconstructions when compared to the actual box-counts $n(b)$, and are not much different than if $p(b, d)$ are calculated by the more accurate method using the angle-of-view from the center of b into d. Due to cost of

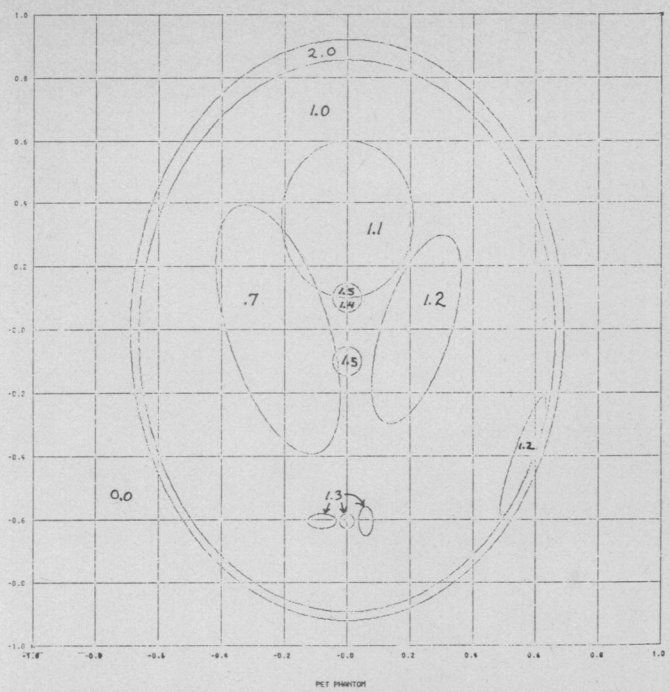

Fig. 2. ET phantom used in the experiments in Section IV. We have modified the phantom of [8] in gray levels to have more contrast and to represent a possible emission density $\lambda(x, y)$. Note, however, that the skull would ordinarily absorb little emitter and has been added simply to define a boundary and for comparison with [8]. C. L. Mallows points out, correctly, that adding the skull as we have done is inadvertently slightly unfair to the convolution–backprojection approach because the artifacts in Figs. 8 and 9 exterior to the skull would not appear for a more relevant phantom.

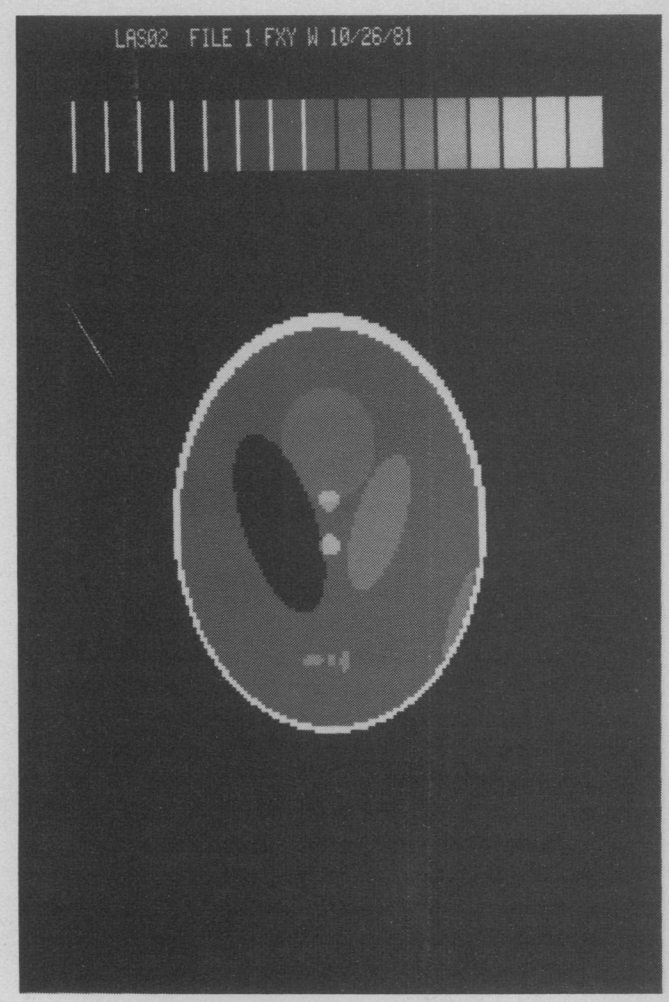

Fig. 3. Photodisplay of Fig. 2.

computation we were unable to use a still more accurate choice for $p(b, d)$ where the emission point is distributed uniformly over b rather than just at the center. However, we are encouraged by the results above that the reconstruction does not depend too critically on the choice of $p(b, d)$ assuming that it is reasonable. We hope to study other more accurate choices for $p(b, d)$. The choice of $p(b, d)$ seems to be less critical than for the ART algorithm of transmission tomography [8] where the corresponding weights are seen to play an important role. It may be that this is because $p((x, y), d)$ vanishes along the sides of the tubes and so even center-weighting does not produce large errors as in [8]. Of course for a more complex or a three-dimensional array of detectors this choice of $p(b, d)$ would be computed once and stored. We feel that our results show that similar quality reconstructions could be expected in any such case.

Of course, (2.13) is not the only way to find a maximum likelihood estimator but is the EM algorithm in this case [5] as we see in Appendix I. We plan to study alternate methods to maximize $l(\boldsymbol{\lambda})$ based on the gradient since this is available from (2.6) and steepest ascent methods would probably be faster [9]. However, properties (2.14) and (2.16) should not be given up lightly.

The present algorithm (2.13) is in several ways reminiscent of the so-called multiplicative ART [6]. However, our choice of constants $p(b, d)$ is certainly different and related to the actual physics of the problem, as we have seen in Section I. Further, our algorithm itself can be derived from the Poisson model as is done in Section II. The algorithm (2.13) has no advantage in transmission tomography, since the use of $(1.6)'$ over (1.6) is then incorrect. It is likely to have advantage over transmission algorithms for emission tomography only at low count rates, or when the geometry of the detector array is so complex that transmission algorithms are hard to obtain.

IV. Simulation Experiments

We study only two-dimensional, or single-ring ET and assume that there are $B = 128 \times 128$ boxes surrounding the unit circle (the patient circle). We assume 128 discrete detectors equally spaced around the circle of radius $\sqrt{2}$ circumscribing the display boxes. We use the phantom in Figs. 2 and 3 with density $\lambda(x, y)$ and choose 10^7 random points from the density $\lambda(x, y)/\iint \lambda$ independently. Each point is chosen by taking a uniform random point in the square $|x|, |y| \leqslant 1$ and accepting it with probability $\lambda(x, y)$. This gives the emission points as if $\lambda(x, y)$ were the true emission density. The histogram of the number of emissions in each box is displayed in Fig. 4. After choosing each point we choose a random line L through the point and increment the count for the detector unit corresponding to the two detector intervals that L passes through. This gives the numbers $n^*(d)$, $d = 1, \cdots, D \approx 64 \times 65$ since there are 65 detector intervals opposite each one. Note that

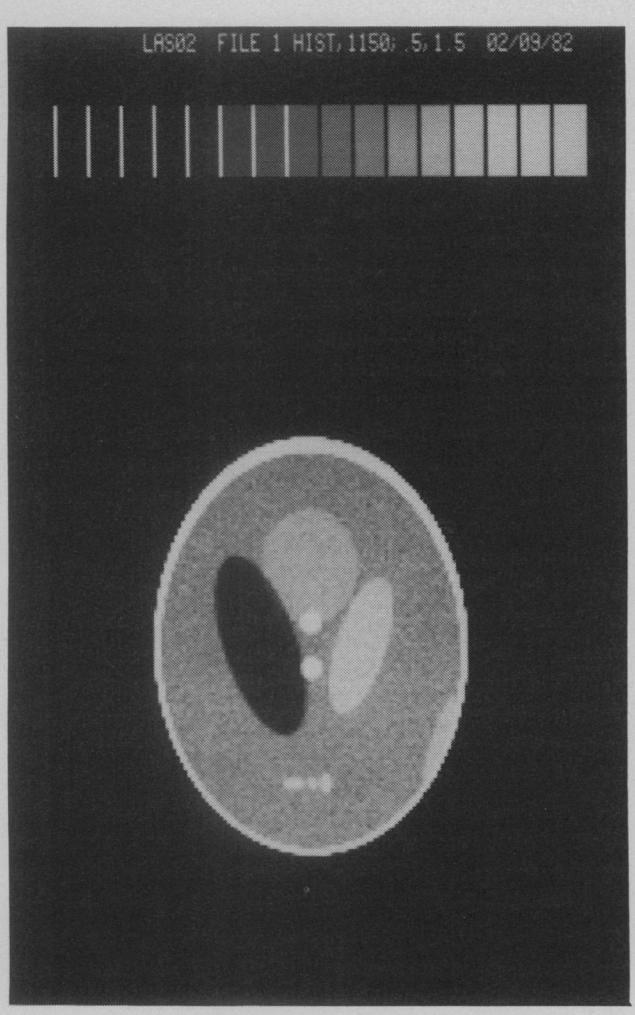

Fig. 4. Histogram $n(b)$ of the 10^7 counts drawn from the phantom of Fig. 2 at a rate proportional to $\lambda(x, y, z)$ at each point. It is felt that 10^7 would be about the right value for single ring positron ET in practice. Of course, without measuring exact time-of-flight, $n(b_0)$ is not observable except in a simulation.

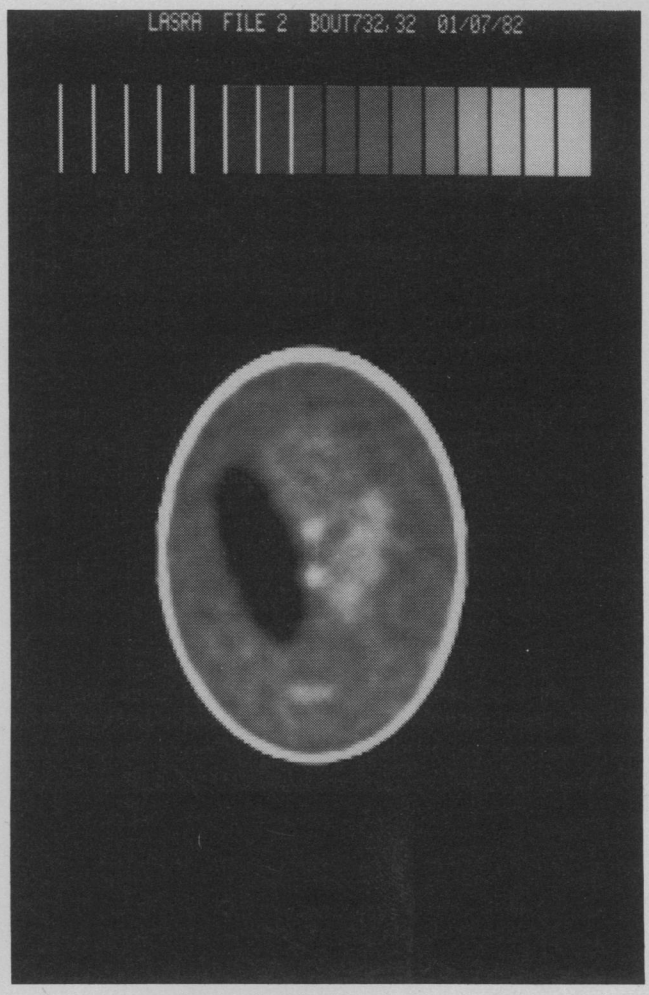

Fig. 5. Reconstruction by (2.13) with $p(b, d)$ as in Section III by the program of Appendix II after 32 iterations.

$B \approx 128^2\ \pi/4$ since boxes outside the unit circle have known emitter density zero.

The data $n^*(d)$ are fed into the computer program in Appendix II which is included for repeatability purposes and the reconstruction (2.13) with 32 iterations is displayed in Fig. 5. It is remarkably accurate as is seen by comparing the numbers on the line plots, Figs. 6 and 7, of the original histogram (Fig. 6) and the reconstruction (2.13) with the constants of the program in Appendix II along the line $y = 0$. The same data $n^*(d)$ are then fed into the usual convolution-backprojection reconstruction in fan-beam configuration [7] with the Lakshminarayanan filter [7]. The reconstruction is displayed in Figs. 8 and 9 and is clearly noisier than that of (2.13) (Figs. 5 and 7). It also has a cupping artifact (the dip close to the skull) which is perhaps due to the error of using (1.6) instead of (1.6)′ as discussed in Section I. Although smoothing with other filters could be used to reduce noise in Figs. 8 and 9 to the level of that in Figs. 5 and 7, we feel that this might result in excessive smoothing. It is interesting that (2.13) is a nonlinear algorithm and smoothing is a linear procedure. The maximum

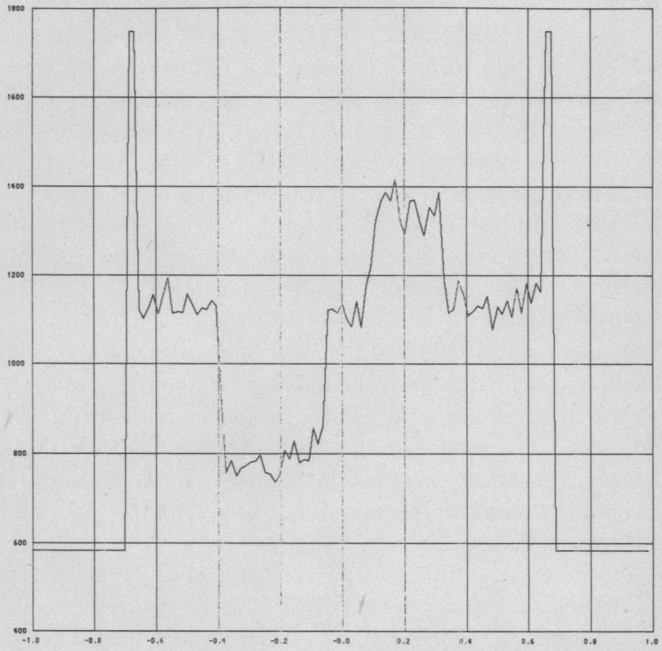

Fig. 6. Line plot of the histogram Fig. 4 through $y = 0$ (the x-axis).

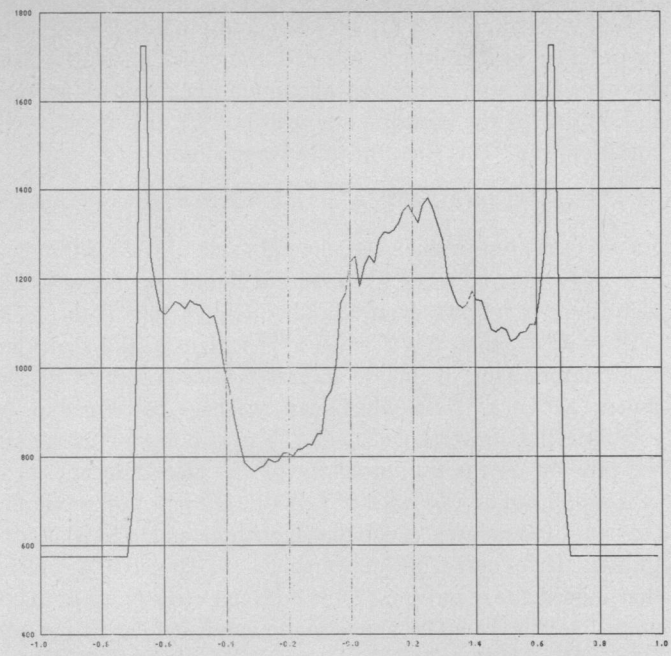

Fig. 7. Line plot of Fig. 5 along $y = 0$ (the x-axis). Note the quantitative agreement between Figs. 6 and 7.

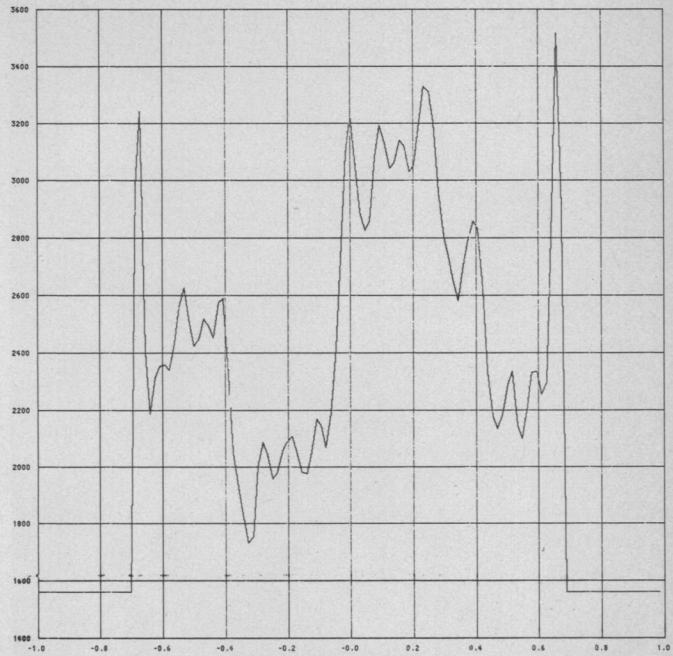

Fig. 9. Line plot of Fig. 8. Here the dip inside the skull is easy to see. Note that the actual numerical values have no significance and some are negative although they have been clipped in this display.

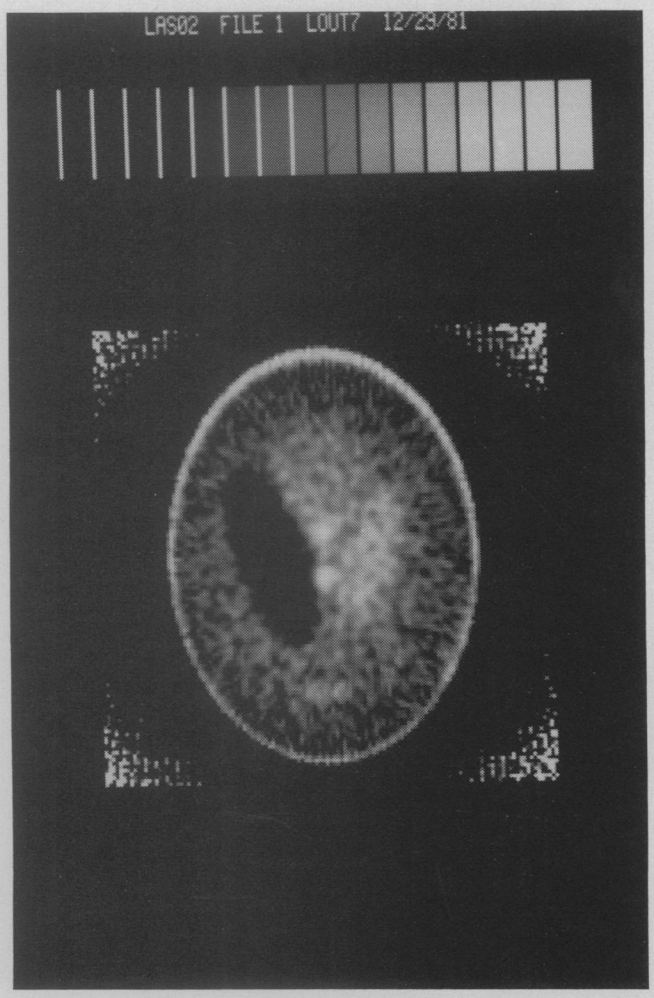

Fig. 8. Reconstruction by convolution backprojection from same data n^*. Note the increased noise and cupping artifact inside the skull.

likelihood estimator thus seems to have good noise suppression over linear algorithms.

In order to test how critical the choice of constants $p(b, d)$ is in (2.13), we took an extreme case where $p(b, d)$ is $1/\pi \times$ (angle of view into detector d from the center of b). This involved an enormous amount of computation because $p(b, d)$ had to be calculated from the relatively complex subroutine determining angle-of-view each time it was needed. The 14th iteration is displayed in Figs. 10 and 11 and are seen to be nearly identical to Figs. 5 and 7. Of course, if $p(b, d)$ could be computed and stored to avoid the need for recomputation, we would expect this choice to be preferable and perhaps uniform weighting in b as discussed in Section III to be still better.

Appendix I

We discuss here the relations between (2.13), the EM algorithm [5], and the Kuhn–Tucker (KT) conditions for optimality [9]. Since $l(\boldsymbol{\lambda})$ of (2.5) is concave, it follows from [9, Theorem 2.19(e)] that sufficient conditions for $\hat{\boldsymbol{\lambda}}$ to be a maximizer of l are the KT conditions which, for our case, turn out to be: for each $b = 1, \cdots, B$,

$$0 = \lambda(b) \frac{\partial l(\boldsymbol{\lambda})}{\partial \lambda(b)}\bigg|_{\hat{\boldsymbol{\lambda}}} = -\hat{\lambda}(b) + \sum_{d=1}^{D} \frac{n^*(d)\hat{\lambda}(b)p(b,d)}{\sum_{b'=1}^{B} \hat{\lambda}(b')p(b',d)} \tag{A1}$$

and

$$\frac{\partial l(\boldsymbol{\lambda})}{\partial \lambda(b)}\bigg|_{\hat{\boldsymbol{\lambda}}} \leqslant 0 \quad \text{if } \hat{\lambda}(b) = 0. \tag{A2}$$

Having such a relatively simple expression for the right side of (A1) [which is derived from (2.6)], one could think of many

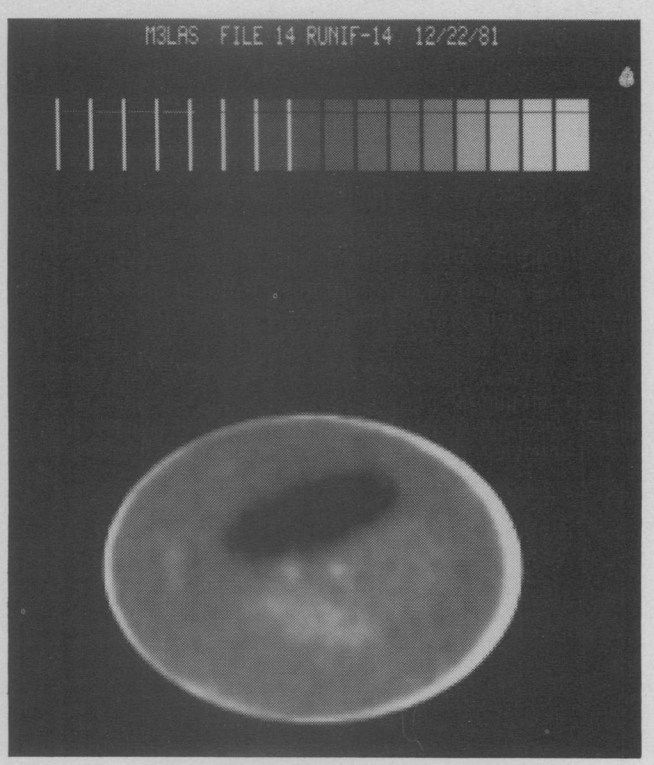

Fig. 10. Reconstruction by (2.13) where $p(b,d) = 1/\pi \times$ angle of view from the center of b into tube d. Almost the same as Fig. 5.

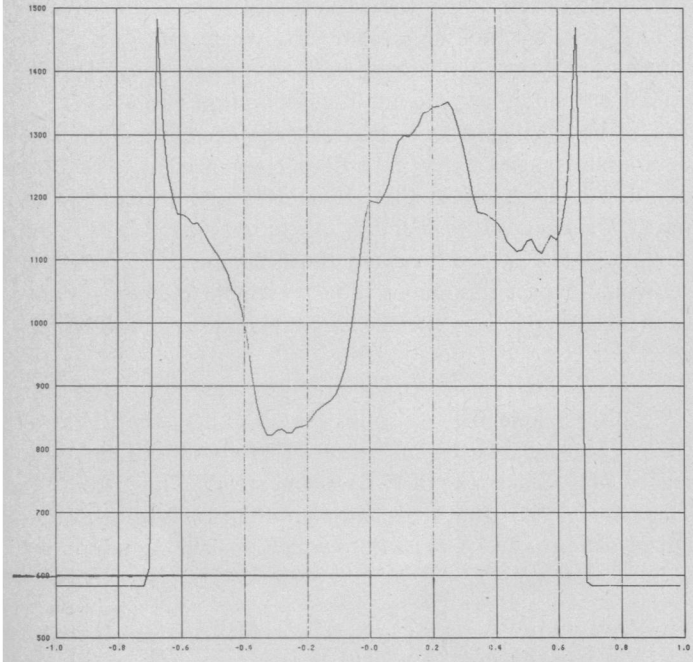

Fig. 11. Line plot of Fig. 10 along $y = 0$ (the x-axis). Almost the same as Fig. 7.

iterative schemes that would converge to a maximum of l. A particularly appealing one is (2.13) because it is a special case of the EM algorithm (E stands for expectation, M for maximization). Here is the rationale behind the EM algorithm, tailored to our example. Had we believed that $\hat{\boldsymbol{\lambda}}^{\text{old}}$ is the true $\boldsymbol{\lambda}$, we would estimate the number of annihilations in box b to be $\hat{n}(b) = E[n(b)|\,\hat{\boldsymbol{\lambda}}^{\text{old}}, \boldsymbol{n}^*]$; this is the expectation step. But, if $\hat{n}(b)$ is our estimate for the emission count in box b we should, in order to be consistent, estimate the emission density $\lambda(b)$ by $\hat{n}(b)$ (because this is the maximum likelihood estimate if indeed $\hat{n}(b)$ is the emission count in box b); this is the maximization step. This gives the iterative scheme

$$\hat{\lambda}^{\text{new}}(b) = E[n(b)|\,\hat{\boldsymbol{\lambda}}^{\text{old}}, \boldsymbol{n}^*] \qquad b = 1, \cdots, B. \tag{A3}$$

As we have seen from (2.10), the right side of (A3) is the right side of (2.13) and so (2.13) is an EM algorithm. Being an EM algorithm, it follows from [5, Theorem 1] that if in (2.13) $\hat{\boldsymbol{\lambda}}^{\text{old}} \neq \hat{\boldsymbol{\lambda}}^{\text{new}}$, then $l(\hat{\boldsymbol{\lambda}}^{\text{old}}) < l(\hat{\boldsymbol{\lambda}}^{\text{new}})$; that is, the algorithm is monotone (the likelihood increases in each step of (2.13), unless $\hat{\boldsymbol{\lambda}}^{\text{old}} = \hat{\boldsymbol{\lambda}}^{\text{new}}$ in which case we have converged). To establish the convergence of (2.13) to a point of maximum we rely on 1) the monotonicity of the algorithm and 2) if $\hat{\boldsymbol{\lambda}}$ is a point of convergence of (2.13) it is a point of maximum (to be proved below). Since the algorithmic map (2.13) is continuous, it follows from convergence [9, Theorem A, p. 91] that indeed the algorithm (2.13) converges to a point of maximum likelihood. (The above argument is similar to the one used in Vardi [10] in another application of the EM algorithm.) To prove 2), we first note that if $\hat{\boldsymbol{\lambda}}$ is a point of convergence then necessarily it satisfies the first KT condition (A1). To see that it also satisfies the second condition (A2), assume (by negation) that there exists a b such that $\hat{\lambda}(b) = 0$ but

$$\left.\frac{\partial l(\boldsymbol{\lambda})}{\partial \lambda(b)}\right|_{\hat{\boldsymbol{\lambda}}} = -1 + \sum_{d=1}^{D} \frac{n^*(d)p(b,d)}{\sum_{b'=1}^{B} \hat{\lambda}(b')p(b',d)} > 0.$$

Now, since $\hat{\boldsymbol{\lambda}}^{(k)} \to \hat{\boldsymbol{\lambda}}$ we get (because of the continuity of $\partial l/\partial\lambda$) that there exists an $\epsilon > 0$ and k_0 such that for all $k > k_0$

$$\sum_{d=1}^{D} \frac{n^*(d)p(b,d)}{\sum_{b'=1}^{B} \hat{\lambda}^{(k)}(b')p(b',d)} > 1 + \epsilon$$

and hence, from (2.13),

$$\hat{\lambda}^{(m+k_0)}(b) \geqslant \hat{\lambda}^{(k_0)}(b)(1+\epsilon)^m \to \infty \qquad \text{as } (m \to \infty)$$

which is a contradiction to (2.16). Note that in the last assertion we assumed $\hat{\lambda}^{(k_0)}(b) > 0$. If this is not the case, so that $\hat{\lambda}^{(k_0)}(b) = 0$, then necessarily b is such that $n^*(d)p(b,d) = 0$ for $d = 1, \cdots, D$, and we get

$$\left.\frac{\partial l(\boldsymbol{\lambda})}{\partial \lambda(b)}\right|_{\hat{\boldsymbol{\lambda}}} = -1 < 0$$

as desired.

Remark: If $\boldsymbol{\lambda} = \boldsymbol{\lambda}^{\text{old}}$ is a solution of (1.14) with n^* substituted for $\boldsymbol{\lambda}^*$, i.e.,

$$n^*(d) = \sum_{b=1}^{B} \lambda^{\text{old}}(b)p(b,d) \qquad d = 1, \cdots, D \tag{A4}$$

then $\boldsymbol{\lambda}^{\text{old}}$ is a stationary point of (2.13). Nevertheless, because of low count rate variations, (A4) would typically be inconsistent, and hence attempting to solve (A4) would be a futile way of deriving a stationary point of (2.13).

APPENDIX II

The following program reconstructs $B = \lambda$ from PNP = n^* from (2.13) iteratively. The array PH keeps the denominator in (2.13) and F is used to hold the numerator before updating B. The constants $p(b, d)$ are calculated as W when needed on the fly. The summation over boxes b is by row or column depending on tube direction being lesser or greater than 45°. The calculation of $p(b, d) = W$ is required in calculating the denominator PH and again in calculating the numerator sum to update $B = \lambda$ in each iteration. The $p(b, d)$ have been chosen so that W is calculable by a few addition and maximization operations as described in Section III. The input count data are read in from file 10, the input λ^0 is read in from file 9, and the reconstruction is written out onto file 11.

```
C POSITRON EMISSION RECON WITH E-M ALGORITHM
C I=(I1,I2) INDEXES THE ITH BOX WITH CENTER AT -1+(2I-1)/(2B-1) I=I1,I2
C B(I)=LAMBDA(I);F(I)=SUM(H(.,K)C(I,K)/PH(K))
C K=(K1,K2) INDEXES THE KTH TUBE WITH CENTERS AT (K-1)2PI/ND
C PNP(K)=NO. COUNTS IN TUBE K; PH(K)=SUM(B(J)C(J,K))
C NC=TOTAL NO. OF COUNTS,ND=NO.DETECTORS,.5ND(ND-1)=NO. TUBES
C T1K,T2K= DISTANCES FROM 0. TO EDGES OF TUBE K, -RD<T2K<T1K<RD
C W=WIDTH OF THE INTERSECTION OF THE KTH TUBE AND THE ITH SPHERE
C RD=RAD. OF DETECTOR CIRCLE DIV. BY RAD. OF PATIENT CIRCLE(=1.)
      PARAMETER (NB=128,ND=128,NC=1000000,ND2=2*ND,NITER=16)
      DIMENSION B(NB,NB),F(NB,NB),PNP(ND,ND),PH(ND,ND)
      DIMENSION X(NB),ST(ND2),CT(ND2)
      INTEGER INH(NB),INX(NB)
C DEFINE CONSTANTS
      RHO=1./NB
      CC=1./(2.*RHO*ND)
      RD=SQRT(2.)
      PI=3.141592654
      PI2=2.*PI
      RNB2=.5*NB
      RNDPI2=ND/PI2
      PI2ND=PI2/ND
      DO 10 I=1,NB
10    X(I)=-1.+(I-.5)*2./NB
      DO 11 K=1,ND2
      TH=.5*(K-1.)*PI2ND
      ST(K)=SIN(TH)
11    CT(K)=COS(TH)
      DO 12 I=1,NB
      R2=SQRT(1.-X(I)*X(I))
      INH(I)=(1-R2)*.5*NB+.5
      INH(I)=MAX0(INH(I),1)
      INX(I)=(1+R2)*.5*NB+.5
      INX(I)=MIN0(INX(I),NB)
12    CONTINUE
      TINY=.5*0.01
      N1=55
      N2=139
C READ THE RAW TUBE DATA
      DO 101 K2=1,ND
      READ(10,1002) (PNP(K1,K2),K1=1,ND)
101   CONTINUE
      PRINT 1002,((PNP(I,K2),K2=1,ND)
1002  FORMAT(10F12.1)
CCCCCCCCCC
C INITIALIZE B TO INPUT FILE
      DO 229 JR=1,2
      DO 231 I2=NB,1,-1
      READ(9,1009) (B(I1,I2),I1=1,NB)
      IF(I2.EQ.N1.OR.I2.EQ.N2)PRINT 1009,(B(I1,I2),I1=1,NB)
231   CONTINUE
229   CONTINUE
1009  FORMAT(10F12.4)
CCCCCCCCCCCCCCCCCCCCCCCCCCCCCCCCCCCCCCCCCCCCCCCCCCCCCCCCCCCCCCCCCCCCCC
      DO 501 ITER=1,NITER
C UPDATE PH(K)=SUM(B(J)*C(J,K))
      DO 301 K1=1,ND-1
      DO 302 K2=K1+1,ND
      PH(K1,K2)=0.
C CK=COS(THK),SK=SIN(THK),THK=(ALF+BET)/2 WHERE X*CK+Y*SK=T1K,T2K DEFINE
C THE EDGE LINE OF TUBE K WITH CENTERS AT RDCOSALF,RDSINALF & AT
C (RDCOSBET,RDSINBET), 0<=ALF<BET<2 PI.
      CK=CT(K1+K2-1)
      SK=ST(K1+K2-1)
      T1K=RD*CT(K2-K1)
      T2K=RD*CT(K2-K1+2)
      DK=2.*RHO
C SKIP IF (X(I1),X(I2)) TOO FAR FROM TUBE K
      IF(ABS(CK).LT.ABS(SK))GO TO 305
C NOW RUN THROUGH BOXES BY ROWS
      DK=2.*RHO
      DO 303 I2=1,NB
      IA=( (1.+(T2K-RHO-X(I2)*SK)/CK)*RNB+1.)*.5
      IB=( (1.+(T1K+RHO-X(I2)*SK)/CK)*RNB+1.)*.5
      I11=MAX0(INH(I2),1+MIN0(IA,IB))
      I12=MIN0(INX(I2),MAX0(IA,IB))
      TIP=X(I11)*CK+X(I2)*SK-DK+RHO
      TIN=TIP-2.*RHO
      IF(I11.GT.I12)GO TO 303
      DO 304 I1=I11,I12
      TIP=TIP+DK
      TIN=TIN+DK
      W=AMAX1(TIP-T2K,0.)+AMAX1(TIN-T1K,0.)-AMAX1(TIP-T1K,0.)
      W=W-AMAX1(TIN-T2K,0.)
      PH(K1,K2)=PH(K1,K2)+W*B(I1,I2)
C     PRINT 1003,K1,K2,I1,I2,I11,I12,PH(K1,K2),W,B(I1,I2),CK,SK
C    &,T1K,T2K,TIP,TIN
C1003 FORMAT(6I4,9F10.4)
304   CONTINUE
303   CONTINUE
      GO TO 302
305   CONTINUE
C NOW RUN THROUGH BOXES BY COLS
      DK=SK*2./NB
      DO 306 I1=1,NB
      IA=( (1.+(T2K-RHO-X(I1)*CK)/SK)*RNB+1.)*.5
      IB=( (1.+(T1K+RHO-X(I1)*CK)/SK)*RNB+1.)*.5
      I21=MAX0(INH(I1),1+MIN0(IA,IB))
      I22=MIN0(INX(I1),MAX0(IA,IB))
      TIP=X(I1)*CK+X(I21)*SK-DK+RHO
      TIN=TIP-2.*RHO
      IF(I21.GT.I22)GO TO 306
      DO 307 I2=I21,I22
      TIP=TIP+DK
      TIN=TIN+DK
      W=AMAX1(TIP-T2K,0.)+AMAX1(TIN-T1K,0.)-AMAX1(TIP-T1K,0.)
      W=W-AMAX1(TIN-T2K,0.)
      F(I1,I2)=F(I1,I2)+W*PH(K1,K2)
C     PRINT 1004,K1,K2,I1,I2,I21,I22,PH(K1,K2),W,B(I1,I2),CK,SK
C    &,T1K,T2K,TIP,TIN
307   CONTINUE
306   CONTINUE
302   CONTINUE
301   CONTINUE
C NOW SET B
      SUM=0.
      DO 331 I2=NB,1,-1
      DO 332 I1=INH(I2),INX(I2)
      B(I1,I2)=B(I1,I2)*F(I1,I2)/CC
      SUM=SUM+B(I1,I2)
332   CONTINUE
      IF(ITER.NE.8.AND.ITER.NE.NITER)GO TO 331
      WRITE(11,1009) (B(I1,I2),I1=1,NB)
      IF(I2.EQ.N1.OR.I2.EQ.N2)PRINT 1009,(B(I1,I2),I1=1,NB)
331   CONTINUE
      PRINT 1101,ITER,SUM
1101  FORMAT(I10,F16.5)
501   CONTINUE
      STOP
      END
```


ACKNOWLEDGMENT

L. A. Shepp is grateful to B. Efron for bringing the EM algorithm to his attention in the context of a discussion on ET. Y. Vardi is grateful to D. Schapira for help in programming.

REFERENCES

[1] T. F. Budinger, S. E. Derenzo, G. T. Gullberg, W. L. Greenberg, and R. H. Huesman, "Emission computer assisted tomography with single-photon and positron annihilation photon emitters," *J. Comput. Assisted Tomogr.*, vol. 1, pp. 131–145, 1977.

[2] Z. H. Cho, J. K. Chan, and L. Eriksonn, "Circular ring tranverse axial positron camera for 3-dimensional reconstruction of radionuclides distribution," *IEEE Trans. Nucl. Sci.*, vol. NS-23, pp. 613–622, 1976.

[3] M. M. Ter-Pogossian, M. E. Raichle, and B. E. Sobel, "Positron

emission tomography," *Scientific Amer.*, vol. 243, pp. 170-181, Oct. 1980.
[4] D. L. Snyder, J. T. Lewis, Jr., and M. M. Ter-Pogossian, "A mathematical model for positron-emission tomography systems having time-of-flight measurements," *IEEE Trans. Nucl. Sci.*, vol. NS-28, pp. 3575-3583, 1981.
[5] A. P. Dempster, N. M. Laird, and D. B. Rubin, "Maximum likelihood from incomplete data via the EM algorithm," *JRSS*, vol. 39, pp. 1-38, 1977.
[6] G. T. Herman, A. Lent, and P. H. Lutz, "Relaxation methods for image reconstruction," *Commun. Ass. Comput. Mach.*, vol. 21, pp. 153-158, 1978.
[7] A. V. Lakshminarayanan, "Reconstruction from divergent ray data," Dep. Comput. Sci., SUNY, Buffalo, NY, Tech. Rep. 92, 1975.
[8] L. A. Shepp and B. F. Logan, "The Fourier reconstruction of a head section," *IEEE Trans. Nucl. Sci.*, vol. NS-21, pp. 21-43, 1974.
[9] W. I. Zangwill, *Nonlinear Programming.* Englewood Cliffs, NJ: Prentice-Hall, 1969.
[10] Y. Vardi, "Nonparametric estimation in renewal processes," *Ann. Statist.*, vol. 10, no. 3, pp. 772-776, 1982.

Collimator Effects in High Resolution X-Ray Computed Tomography

JACQUES G. VERLY

Abstract—**This paper complements other studies in the field of image restoration in X-ray computed tomography by including the source collimator among the sources of image degradation. The overall blur is describable in terms of a space variant 2-D impulse response or point spread function, which is initially calculated for an arbitrary scanning eccentricity, a uniform source intensity distribution, a uniform detector sensitivity, and arbitrary collimator aperture and position, and subsequently derived for more complicated sources and detectors. Numerous 3-D hidden-line displays are used throughout to illustrate the complicated 2-D functions emerging from the analysis.**

Introduction

THE PROBLEM of image restoration naturally arises in X-ray computed tomography because the scans recorded at various angular positions are not really sets of pure line integrals, but rather collections of integrals over strips in the isolated slice being imaged. Describing the blur which results from using those data as ingredients in some version of the Radon inversion formula [1] has been the object of a number of recent studies [2]-[7], but actual examples of restoration, even on synthetic data, are not yet available. The most elaborate of these studies take into account various sources of image degradation such as the nonlinearity which characterizes X-ray attenuation measurements, the spatial variation in X-ray intensity across the source, the structure of the detector, and the scanning eccentricity. However, they all implicitly assume that the *collimators* usually inserted near the source and detector have no influence whatsoever on the imaging process. This is not generally true in practice because the set of X-rays reaching the detector is often "pinched" by the *source collimator* in order to increase the dose effectiveness. Very often, however, the *detector collimator* is just wide enough to prevent any additional pinching of the imaging beam. As a result the attention will here be focused on geometries in which a *single* collimator effectively disturbs the imaging process (Fig. 1).

In spite of their abilities to deal with a wide variety of image degradations, this and other related studies [2]-[7] still appear quite ideal since they all assume that the X-ray photon trajectories are strictly confined to the plane of the slice of interest. This is not at all the case in practice and the problem of high resolution tomographic imaging really calls for a true 3-D treatment, as explained in [8]. This recent study, however, has shown that many of the 2-D results could be easily extended to 3-D: in fact, if the theory in [8] is reformulated to take into account the presence of a 2-D collimator, it rapidly becomes clear that the results of the simplified 2-D situation discussed in this paper are also immediately applicable to its direct 3-D counterpart. Since much can be learned and derived from an ideal 2-D analysis, and since the related notations and figures are much simpler, the rest of the paper will focus exclusively on the planar geometry described above.

Manuscript received April 5, 1982; revised July 7, 1982. This work was begun when the author was with the Department of Electrical Engineering, Stanford University, Stanford, CA, and was completed at MIT Lincoln Laboratory with the support of the U.S. Department of the Air Force.

The author is with the Lincoln Laboratory, Massachusetts Institute of Technology, Lexington, MA 02173.

0278-0062/82/1000-0122$00.75 © 1982 IEEE